Cement & Concrete Composites 33 (2011) 1–11

Contents lists available at ScienceDirect

Cement & Concrete Composites

journal homepage: www.elsevier.com/locate/cemconcomp

Mechanical behaviour of strain hardening cement-based composites under impact loading

Viktor Mechtcherine [a,*], Oliver Millon [b], Marko Butler [a], Klaus Thoma [b]

[a] Institute for Construction Materials, TU Dresden, Germany
[b] Fraunhofer Institute for High-Speed Dynamics, Ernst-Mach-Institut, EMI, Freiburg, Germany

ARTICLE INFO

Article history:
Received 19 June 2010
Received in revised form 23 September 2010
Accepted 24 September 2010
Available online 1 October 2010

Keywords:
SHCC
Uniaxial tension
Impact

ABSTRACT

This paper describes the material behaviour of a strain hardening cement-based composite (SHCC) at high strain rates. The results of highly dynamic spall experiments using a Hopkinson bar at strain rates 140–180 s^{-1} are arrayed against the results of quasi-static uniaxial tensile tests at strain rates of 0.001 s^{-1}. This comparison is based on the values of tensile strength, Young's modulus, and fracture energy of the specimens. In addition, the experimental results of SHCC are related to the characteristic values of other concrete types. Differences in material behaviour are explained by the phenomena of crack formation and fibre pullout resistance.

1. Introduction

Strain hardening cement-based composites (SHCC) are cementitious materials which show an increase in load-bearing capacity after the formation of the first crack when subjected to uniaxial tensile loading, cf. Fig. 1. Strain hardening is accompanied by pronounced multiple cracking, which leads to the quasi-ductile behaviour of the composite. The crack-bridging load transfer is ensured by the addition of short fibres to the concrete matrix.

The generation of numerous new crack surfaces and the distinct, gradual pullout of crack-bridging fibres allow very high energy absorption under quasi-static as well as under dynamic tensile loads [1,3]. These features enable the application of SHCC in the strengthening of structures exposed to sudden mechanical loading with high energy content (e.g. impact or detonation). Also, the building of new structures with enhanced impact resistance is possible using SHCC.

The excellent mechanical performance of SHCC has been demonstrated numerous times in the case of quasi-static loading (e.g. [1,2]). There is, however, much less information on the effect of increased strain rates on the load-bearing behaviour of such composites. Yang and Li [3] reported a pronounced increase in first-crack stress and tensile strength of SHCC made with PVA fibres (PVA – Polyvinylalcohol) with increasing strain rates. The strain rates varied from 10^{-5} s^{-1} to 10^{-1} s^{-1}. At the same time the strain capacity (i.e. the strain measured on reaching the tensile strength of the composite) decreased, but multiple cracking of the SHCC could still be observed. Yang and Li showed that the strain rate sensitivity of the highly ductile SHCC under investigation was directly influenced by the morphology of the interface between fibre and cementitious matrix (type and shape of hydration products, structural density of hydration products etc.). In demonstrating this dependency they performed pullout tests and measured chemical bond strength. When the pullout speed rose from 10^{-3} mm/s to 10 mm/s, in terms of specific energy the strength of the chemical bond increased from approximately 1 J/m^2 to 5 J/m^2. Douglas and Billington [4] investigated less ductile SHCC at strain rates between 2×10^{-5} and 2×10^{-1} s^{-1}. The general tendency of the results of that study was similar to the findings publicised by Yang and Li [3], however, multiple cracking was present only at quasi-static loading. Maalej et al. [5] reported a minor influence of interface morphology on the strain rate sensitivity of SHCC when the fibres had no chemical bond to the matrix. Their tests were performed at strain rates ranging from 2×10^{-6} to 2×10^{-1} s^{-1}. Boshoff et al. [6] performed pullout tests on single PVA fibres and varied the pullout speed between 10^{-2} and 10^{2} mm/min. An increasing pullout resistance was stated already at these relatively low rates with rising pullout velocity. An increased probability of fibre failure instead of fibre pullout was noticed at the same time.

This paper presents the results of short-time dynamic measurements on a particular SHCC composition at strain rates 140–180 s^{-1}, which is considerably higher than the strain rates used in each of the previous investigations. The dynamic experiments were performed by means of a Hopkinson bar. Uniaxial, quasi-static tensile tests served as reference. The mechanical performances

* Corresponding author. Tel.: +49 351 463 35 920; fax: +49 351 463 37 268.
E-mail address: mechtcherine@tu-dresden.de (V. Mechtcherine).

0958-9465/$ - see front matter © 2010 Elsevier Ltd. All rights reserved.
doi:10.1016/j.cemconcomp.2010.09.018

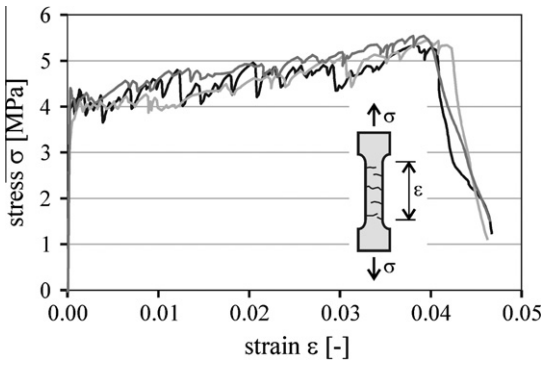

Fig. 1. Typical stress–strain curves of SHCC.

under dynamic and quasi-static loadings are compared and also related to the observed crack patterns and the condition of fracture surfaces.

2. Experimental program

2.1. General remarks

Cylindrical samples with identical geometry and material composition were used to determine SHCC mechanical performance in both the high-speed dynamic tests (Hopkinson bar) and quasi-static tests. The determination of the Young's modulus and the tensile strength was performed using unnotched cylinders, whereas the measurement of the fracture energy was performed on notched samples. All investigations were accomplished at a sample age of 28 days. In the following sections the SHCC composition, the sample production and the experimental setup for the quasi-static and dynamic tests as well are described.

2.2. Mix design and mixing of SHCC

The excellent mechanical behaviour of SHCC is achieved by specific adjustment of the characteristics of the cementitious matrix, crack-bridging fibres, and the bond between matrix and fibres. To guarantee the pronounced ductile material behaviour and, hence, the high energy absorption, the following conditions must be satisfied [1,2]:

- sufficiently high-fibre-volume content in order to insure the transfer of tensile stresses higher than the first- crack stress of the composite, thus enabling the multiple cracking of SHCC. This stress transfer over the crack has to be assured despite the nearly random fibre orientation in the matrix volume;
- progressive debonding in the fibre–matrix interface and subsequent pullout of crack-bridging fibres, in which the pullout force should be as high as possible;
- ductile material behaviour of fibres as well as their insensitivity to lateral pressure in order to enable the participation of non-orthogonally oriented fibres in crack-bridging and fibre pullout;
- uniform distribution of fibre in the matrix volume; and
- presence of numerous, well distributed crack initiators (micro-defects) to promote finely distributed, multiple cracking.

The SHCC examined in the experiments presented was developed at the Institute of Construction Materials at the TU Dresden considering the aspects mentioned above. Furthermore, specific requirements concerning freeze–thaw resistance of the material were investigated [7]. The fibre volume content of this SHCC was 2.2% by volume. The synthetic PVA fibres were produced by Kuraray (Japan). The diameter of the fibre was approximately 40 μm and the cut length 12 mm. The relatively high-fibre-volume content required a very finely grained matrix composition to guarantee good workability of the fresh SHCC and uniform distribution as well as random orientation of fibres. Accordingly the maximum particle size of the aggregates was only 0.2 mm. The binder content was very high in comparison to ordinary concrete, the binder being composed of cement CEM I 42.5 R and fly ash. On the one hand the high portion of fly ash assured good workability of the fresh SHCC. On the other hand the fly ash particles acted as crack initiators in the hardened matrix. The spherical SAP particles (SAP – Super Absorbing Polymer) acted in the same way. The SAPs absorb high amounts of water and swell. During cement hydration swollen particles release the absorbed water as a result of the capillary action of the hardening matrix. In consequence, spherical cavities of diameter up to 500 μm remain in the cementitious matrix, triggering micro-crack initiation at great number of spots. Beyond that SAP particles also mitigate shrinkage and enhance the freeze–thaw resistance of the SHCC matrix favourably [7]. Table 1 gives the composition of the SHCC.

The production of fresh SHCC was accomplished as follows: All dry components (without fibre) were homogenized in the mixer. Then the water with 50% superplasticizer was added and mixed until a low-viscous, fluid consistency was achieved. Subsequently the fibre was added gradually during continuous mixing. Afterwards the composition was mixed intensively until a uniform fibre distribution was reached. Finally, the remaining portion of superplasticizer was added to adjust the desired consistency of fresh SHCC.

2.3. Geometry and production of specimens

When filling fresh SHCC into formwork, the fibres in the zones near the surface are predominantly oriented parallel to the formwork walls (the so-called wall effect). In order to guarantee random fibre orientation in the entire sample volume, cylindrical specimens were extracted from the large SHCC blocks by core drilling. The distance between the lateral surfaces of the drilled cylinders and the outer surfaces of the SHCC blocks was 30 mm. At the top and bottom of the cylinders the distance to the block surfaces was approximately 40 mm.

The diameter of the cylindrical specimens was $D = 75$ mm and their length $L = 250$ mm. The notched samples were notched around their circumferences (Fig. 2b). The width of the sawed notch was 2 mm, its depth 18 mm. The core drilling as well as plane grinding of the cylinders took place at a concrete age of 7 days. Before and after the cutting of the specimens, the blocks or samples were sealed by wrapping them in plastic foil to prevent drying the SHCC.

2.4. Quasi-static tensile test: test setup and method of data evaluation

In performing the uniaxial tensile tests, the cylindrical specimens were glued in special steel-made sample holders. The

Table 1
Matrix composition of SHCC (kg/m^3).

CEM I 42.5 R-HS	505
Fly ash	614
Water	334
Sand 0.06–0.2 mm	534
Stabiliser	3.2
SAP	2.0
Superplasticizer (PCE)	9.5
PVA fibre	29.3

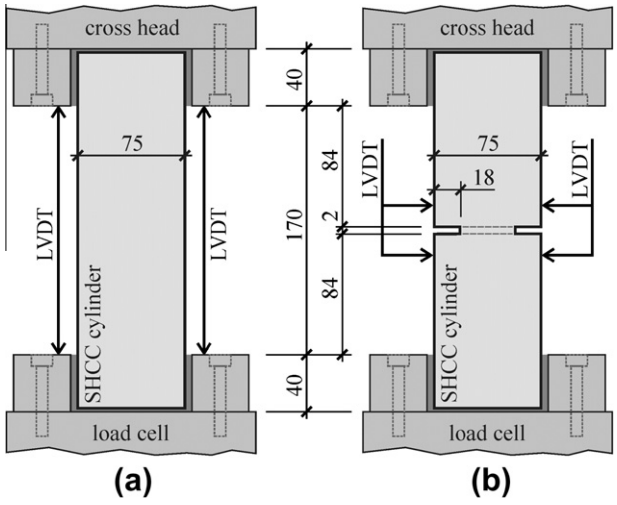

Fig. 2. Quasi-static tensile test setup for SHCC cylinders without notch (a) and with notch (b).

bonding length was 40 mm at the foot as well as at the head of each sample. The upper sample holder was fixed so as not to rotate at the cross head of the testing machine (type: Zwick Z1200, max. Load 1200 kN). The lower sample holder was fixed at the top of the load cell, also so as not to rotate. In order to guarantee a restraint-free initial specimen condition, the gluing of the foot end of the sample occurred directly in the testing machine after fixing the head of the specimen to the cross head.

The free length between the sample holders was 170 mm. The absence of a narrowed zone in unnotched specimens (e.g. dumb-bell shape, customarily used in SHCC testing) carries generally with it an enhanced probability of first cracking in the vicinity of the sample holder due to stress concentrations. Thus, the deformation of unnotched cylinders was measured between the sample holders by means of two LVDT (Fig. 2a). The tests were performed in a deformation-control regime with a strain rate of 0.001 s^{-1}.

When notched cylinders are used in initiating and widening cracks, cracking is limited to the notched area. Accordingly the deformation was measured by means of two LVDT spanning the notch with a measuring length of 50 mm (Fig. 2b). These tests were executed in a displacement-control regime with a deformations rate of 0.01 mm/s.

The measured data recorded in the tensile tests on unnotched cylinders was evaluated to derive Young's modulus, the tensile strength, and the total fracture energy (also often referred to as "work to fracture" or "work of fracture"). The specific fracture energy, i.e. the total fracture energy related to the total surface of all cracks, could not be computed because of the non-quantified crack state inside the specimen's volume. Some cracks do not span the entire cross-section of the specimen, but end inside the volume.

For notched cylinders the data evaluation was performed to measure the tensile strength and specific fracture energy. The specific fracture energy was determined by relating the total fracture energy to the net area of the notched cross-section of specimen. In addition to the mechanical tests, characteristic phenomena of interaction between fibre and matrix were studied using microscopic images of fracture surfaces and individual fibres after testing.

2.5. Hopkinson bar experiments: test setup and method of data evaluation

High-speed loading is characterized by shock loads, which act on structures for a short time and cause very high compressive and tensile stresses. In such cases of dynamic loading, which arise characteristically out of detonations and impacts, a loading pulse is generated. This pulse propagates from the loaded side of the specimen to the opposite side through the material and reflects there because of the differing impedances. The superimposition of the reflected loading wave onto the second reloading wave leads to dynamic tensile stresses in the material. If the tensile stress is greater than the material's tensile strength, damage to the material will occur. Through the crack initiation and the crack growth, energy can be dissipated, influencing dynamic material behaviour.

With the help of Hopkinson bar experiments, such dynamic loads can be investigated. An ideal uniaxial stress state can be accomplished as shown by Weerheijm [8], Schuler [9] and Millon et al. [10]. At the Fraunhofer Institute for High-Speed Dynamics, Ernst-Mach-Institut (EMI), such experiments are carried out by employing the spallation configuration of Hopkinson bar experiments. In that, the specimen is fixed on the end of the Hopkinson bar's incident bar (Fig. 3).

The load is generated by the shot of the striker bar on the incident bar. The loading pulse generated consists of both a compression wave and a decompression wave propagating through the incident bar. The compression wave is generated through the impact of the projectile. The decompression wave results from the reflection of the compression wave on the projectile's free end (Fig. 4I). Due to the similar impedances of the incident bar and the specimen material, a large portion of the loading pulse is transmitted into the specimen. A small portion is reflected at the boundary surface between bar and specimen (Fig. 4II). The compression wave reaches the specimen's free end first and is completely reflected into a decompression wave there (Fig. 4III). Due to the superimposition of the reflected compression wave onto the

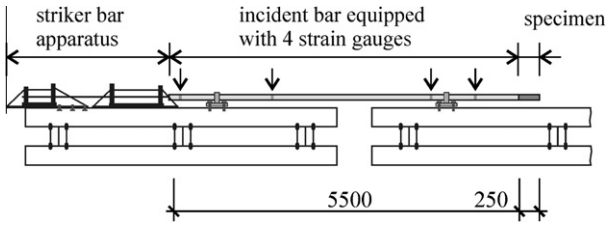

Fig. 3. Sketch of Hopkinson bar in spallation configuration.

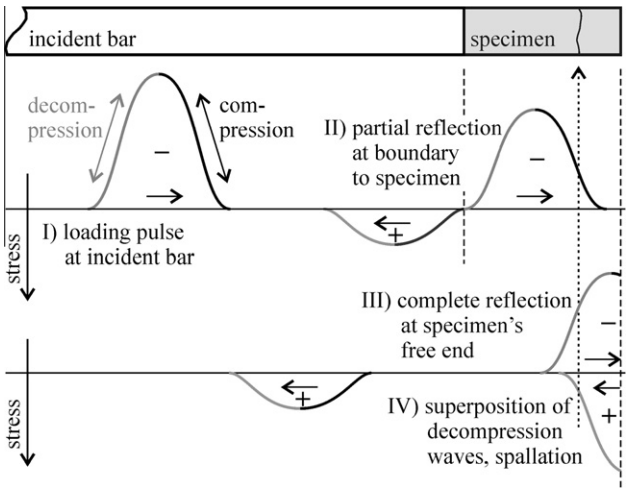

Fig. 4. Loading situation in spallation experiments: Stress wave propagation in the Hopkinson bar and the specimen.

outgoing decompression wave, high tensile stresses occur in the specimen, leading to tensile failure if the material's tensile strength is reached (Fig. 4IV). Material failure is visible in a development of one or more spallation planes. There, the specimen is fragmented into two or more pieces (spallation) [9,11].

With the help of spallation experiments, dynamic Young's modulus, dynamic tensile strength, and dynamic fracture energy can be analyzed. Depending on the properties investigated, notched and unnotched specimens are employed (Fig. 5).

Spallation experiments should only be carried out on materials which have much lower tensile strength than compressive strength [11]. It is necessary that the load with the compressive wave does not cause structural damage, which consequently leads in the spallation experiments to both inexactness and compressive damage. To determine dynamic Young's modulus and dynamic tensile strength, the longitudinal wave propagation velocity must be known in the SHCC specimen. An undisturbed, uniaxial spreading of the loading pulse (incident shock wave) is required. Therefore, it is advisable to determine the wave propagation velocity on unnotched specimens. This calculation is accomplished with the help of the measurement technique attached to the specimen, such as strain and acceleration gauges (Fig. 5). With these it is possible to measure the time of wave propagation between the measurement points Δt (Fig. 6). Dynamic Young's modulus is based on the theory of wave propagation in elastic materials and is calculated with the help of the wave propagation velocity CL and the material's density ρ (Eq. (1)):

$$E_{dyn} = \rho \cdot c_L^2 \tag{1}$$

To calculate the dynamic tensile strength (Eq. (2)), the pullback velocity must be known as well. Pullback velocity Δu_{pb} is the reduction of the free surface velocity on the specimen's free end during the spallation process. The calculation can be done by integrating the acceleration-time signal (Fig. 6).

$$f_{t,dyn} = \frac{1}{2}\rho \cdot c_L \cdot \Delta u_{pb} \tag{2}$$

Dynamic fracture energy is analyzed on notched specimens. The calculation is based on the momentum conservation from the momentum transfer in the spallation plane [9,11,12]. The notch is required to guarantee a complete fragmentation of the specimen in a defined spallation plane to avoid multiple cracking with more than one spallation plane and to fix the optical measurement equipment. Due to reflections, the notch causes a three-dimensional stress state in the material, which results in a reduction of the wave amplitude and a minor change in wave shape. This leads to inexact results and a larger scattering of the values of Young's modulus and tensile strength (see Table 4).

Momentum transfer on the spallation plane I_{1-2} is determined from the change in the momentum of fragment 2 of the specimen (Fig. 5, Eq. (3)). m_2, $v_2(t_1)$, and $v_2(t_2)$, indicating the mass of the free-end fragment and its velocities before (index t_1) and after (index t_2) crack initiation, respectively.

$$I_{1-2} = I_{2(t1)} - I_{2(t2)} = m_2(v_{2(t1)} - v_{2(t2)}) \tag{3}$$

Fig. 7 illustrates the spallation process. The time points required for the calculation of the fracture energy, the fragments resulting from the loading, and their terms of mass and velocity are shown.

Mean crack-opening velocity $\delta_{1-2'}$ is calculated with the help of the velocity differences of both fragments before and after fragmentation (Eq. (4)):

$$\dot{\delta}_{1-2} = \frac{1}{2}(v_{2(t2)} + v_{2(t1)}) - \frac{1}{2}(v_{1(t2)} + v_{1(t1)}) \tag{4}$$

The analytical calculation of the fragments' velocities before spallation is based on the linear wave theory in elastic materials. During and after spallation, determination of the fragments' velocities can be accomplished with the help of a high-speed extensometer to record the displacement–time histories of the respective fragments (see Fig. 5b).

With the results of Eqs. (3) and (4), total dynamic fracture energy G_f can be calculated by using Eq. (5). Specific fracture energy G_f' takes the reduced specimen diameter in the spallation plane into consideration (Eq. (6)).

$$G_f = I_{1-2} \cdot \dot{\delta}_{1-2} \tag{5}$$

$$G_f' = \frac{I_{1-2} \cdot \dot{\delta}_{1-2}}{A_{net}} \tag{6}$$

In addition to fracture energy, dynamic Young's modulus and dynamic tensile strength on notched specimens as well were calculated using Eqs. (1) and (2) for the sake of comparison.

With the help of computer-tomographical analysis, some specimens were investigated with regard to crack propagation in the specimen. Additionally, microscopic analysis of failure surfaces and fibre surfaces were made, describing phenomena in the fibre–matrix interactions.

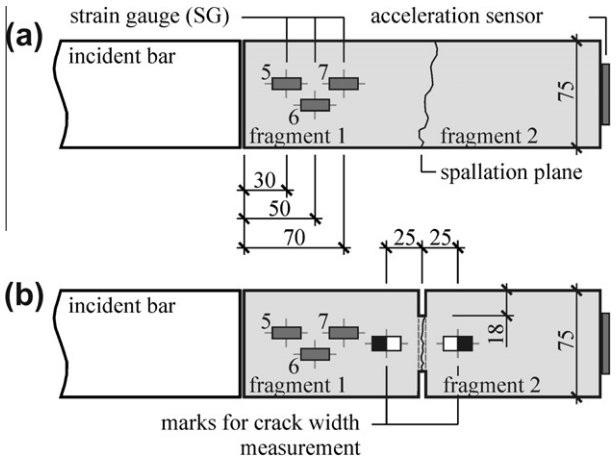

Fig. 5. Instrumentation of SHCC cylinders without notch (a) and with notch (b) on the Hopkinson bar.

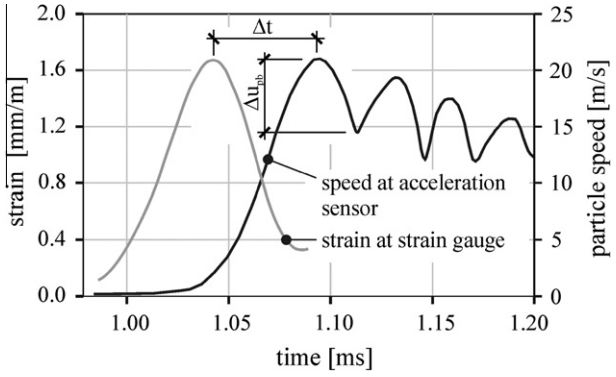

Fig. 6. Determination of wave transition time Δt and pullback velocity Δu_{pb} (example).

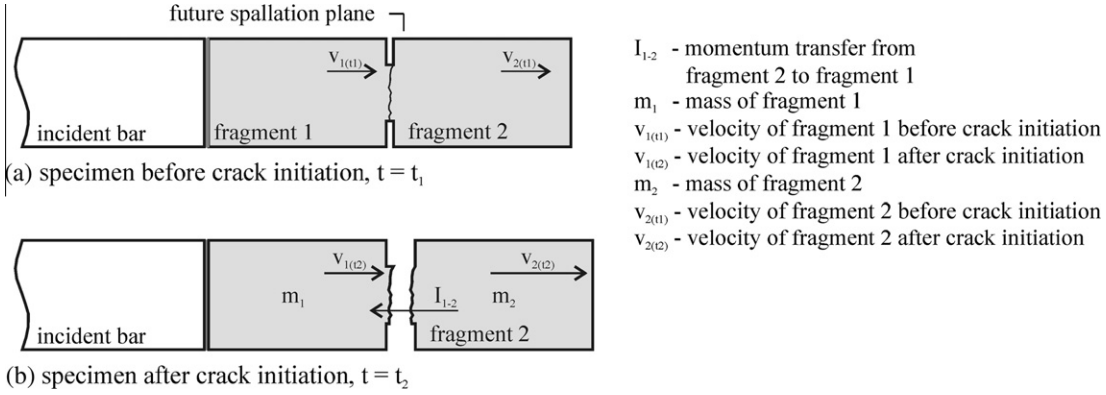

Fig. 7. Schematic description of the spallation process with parameters required to determine the fracture energy.

3. Experimental results

3.1. Results of quasi-static tensile testing

The quasi-static tests were performed at an SHCC-age of 28 days. The compression strength was determined on two specimen geometries: cubes (edge length 100 mm) and cylinders (diameter 75 mm, length 250 mm), where three specimens were tested in each series. The average value of the compressive strength of SHCC was 59.4 MPa for cubes and 60.7 MPa for cylinders, respectively (cf. Tables 2 and 3). Young's modulus was measured on three cylindrical specimens (diameter 75 mm, length 250 mm) according to DIN EN 18555. The gauge length for deformation measurement was 70 mm. The mean value of Young's modulus was 20.6 GPa.

Fig. 8 shows the stress–strain curves obtained from six uniaxial tension tests on unnotched cylinders according to the setup described in Section 2.4. All six tests were performed under the same conditions. First cracking occurred at a stress level between 3 and 4 MPa. Distinct multiple crack formation could be observed on specimen surfaces with increasing strain. At the same time a slight hardening of the composite material was recorded. The cracks formed mainly orthogonally to the direction of the tensile load (Fig. 9). The average tensile strength was 3.8 MPa. The strain capacity scattered notably between approximately 1% and 3%. The different tail shapes of the curves result from the pronounced differences in the statistic fibre distributions and their orientation in the SHCC specimens. The fibre distribution and orientation strongly influence the crack formation (number and shape of cracks) and, with that, the mechanical performance of the SHCC. The failure of the composite was marked by increasing localisation of the crack generation and crack widening of one major crack. The widths of cracks outside the major crack plane decreased while tensile stress decreased in the softening regime (cf. Fig. 9).

In the tensile tests performed on cylinders, the ductility of the cylindrical specimens was smaller than that of the dumbbell shaped specimens made of the same material (cf. Figs. 8 and 1). There are mainly three causes for this. Firstly, the cylinders were core-drilled from a large block. Thus, the fibres positioned at the surface at core-drilled cylinders were randomly oriented and cut.

Table 2
Compression strength and bulk density measured on SHCC cubes (mean value, standard deviation given in parentheses).

Bulk density ρ cube (kg/m^3)	1910 (11)
Compressive strength $f_{c,stat,cube}$ (MPa)	59.4 (1.1)

Table 3
Results of quasi-static tests on SHCC cylinders without and with notch (mean values, standard deviations given in parentheses).

	Without notch	With notch
Bulk density ρ (kg/m^3)	1897 (13)	1897 (13)
Young's modulus (compression) $E_{c,stat}$ (GPa)	20.60 (0.36)	–
Young's modulus (tension) $E_{t,stat}$ (GPa)	9.32 (0.89)	–
Compressive strength $f_{c,stat}$ (MPa)	60.7 (1.0)	–
Tensile strength $f_{t,stat}$ (MPa)	3.80 (0.42)	5.53 (0.29)
Total fracture energy $G_{f,stat}$ (Nm)	61.0 (18.8)	6.69 (1.14)
Specific fracture energy $G_{f,stat}'$ (N/m)	–	5561 (943)

Table 4
Results of Hopkinson bar experiments on SHCC cylinders with and without notch.

	Without notch	With notch
Bulk density ρ (kg/m^3)	1889 (5)	1893 (7)
Wave velocity C_L (m/s)	3571 (61)	3369 (121)
Youngs' modulus E_{dyn} (GPa)	24.1 (0.8)	21.5 (1.6)
Tensile strength $f_{t,dyn}$ (MPa)	25.7 (0.6)	26.6 (6.6)
Crack-opening velocity δ' (m/s)	–	9.03 (0.60)
Specific fracture energy $G_{f,dyn}'$ (N/m)	–	13,316 (2191)

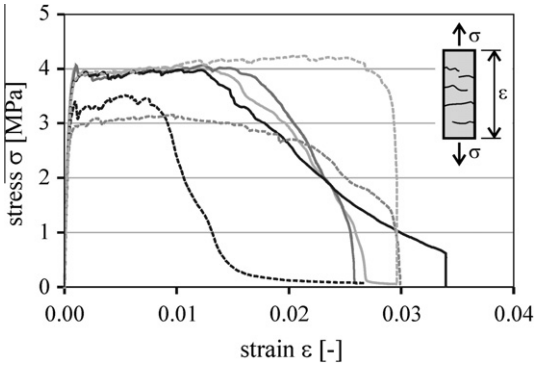

Fig. 8. Stress–strain curves of unnotched SHCC cylinders.

In contrast to this, the surfaces of the dumbbell shaped specimens were defined by the formwork geometry. Here no fibres were cut and the fibre orientation at the specimen surface was parallel to the surface and hence aligned with the loading direction. It should also be mentioned that the dumbbell specimens had a rather slender cross-section of only 24 mm × 40 mm, which also influenced the orientation of the fibres in the direction of loading and thereby leading subsequently to their better mechanical performance.

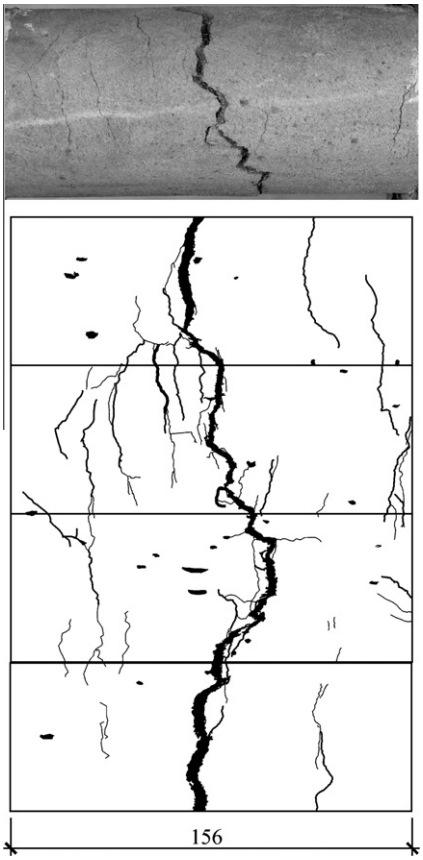

Fig. 9. Wind-off of crack pattern of an unnotched SHCC cylinder after exceeding the failure strain.

Secondly, the constant cross-section of the cylinders (no dumbbell shape) leads to stress singularities close to the glued specimen ends. Therefore, a premature localisation of failure is likely in this region (see also [13]). Finally, it should be considered that the strain rate of 0.001 s^{-1} used in this study for quasi-static experiments was considerably higher that the strain rate of 0.00005 s^{-1} used in another study [7], in which the material composition was developed. As shown in [14], the ductility of SHCC decreases with the increasing strain rate in the quasi-static loading regime. This issue will be addressed again in Section 4.2 when discussing the failure particularities of SHCC.

The total fracture energy $G_{f,stat}$, derived from the area under the tensile stress–strain curve, yielded large scattering about the mean value of 61 Nm (Table 3). As mentioned before, the calculation of a specific fracture energy G'_f, stat by division of the total fracture energy by the total crack surface was not possible. Due to the complex shape of the cracks (cf. Fig. 9) and the widely unknown crack pattern inside the cylinders, the total crack surface could not be determined. The Young's modulus for the tensile loading was determined within the nearly linear elastic range of stress–strain curve with the lower stress σ_u of 0 MPa and the upper stress σ_o of 2 MPa. The average modulus obtained from six specimens was 9320 MPa (Table 3).

Fig. 10 shows the stress–strain curves obtained from six tensile tests on notched cylinders according to the setup described in Section 2.4. In these tests crack initiation takes place only in the notched area at stress levels between 4 and 5 MPa. After crack initiation the tensile stress increases distinctly with increasing crack opening. The average tensile strength of 5.53 MPa (Table 3) was reached at the average deformation of approximately 0.6 mm. Subsequently, a softening of the composite could be observed. The

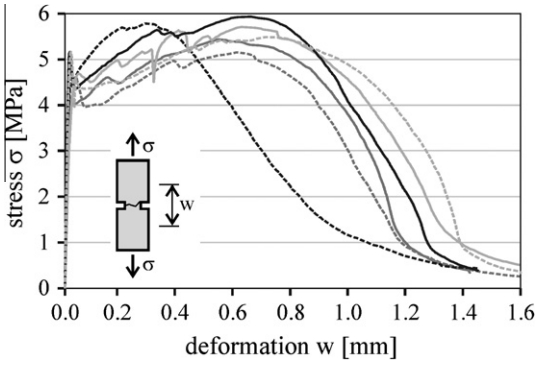

Fig. 10. Stress-deformation curves obtained from uniaxial tension tests on notched SHCC cylinders.

mean value of the total fracture energy $G_{f,stat}$ was 6.7 Nm, while the specific fracture energy $G'_{f,stat}$ was 5661 N/m (Table 3).

3.2. Results of Hopkinson bar experiments

With the help of the spallation configuration of the Hopkinson bar, 13 specimens were tested. The results of the experiments on six unnotched and five notched specimens were used for further evaluation. The mean longitudinal wave propagation velocity was 3571 m/s.

Corresponding to the theoretical foundations stated in Section 2.5, a dynamic Young's modulus of 24.1 GPa and a dynamic tensile strength of 25.7 MPa were observed for unnotched specimens (Table 4). The scattering of both properties is low. On notched specimens as well both properties were measured. The dynamic tensile strength was not only higher (26.6 MPa), but it yields significantly greater scattering as well. The wider scattering can be attributed to the arrangement of the notch, as stated in Section 2.5. A state of three-dimensional stresses is generated in the material due to reflections on the notch. The wave shape and the wave propagation velocity are influenced significantly (Table 4), which causes considerable scattering. The total fracture energy was determined on notched specimens only. Related to the fracture surface, the specific fracture energy reaches a value of 13,300 N/m (Table 4). A great degree of scattering was observed for this property as well.

The unnotched specimens showed multiple crack distribution following the experiment. The primary crack appears in the spallation plane. Its direction is oriented mainly orthogonally to the loading direction, cf. Fig. 11. In addition to the primary crack, many secondary cracks could be detected on the specimens' surfaces. These secondary cracks were mostly parallel to the loading direction. Fig. 11 shows a typical wind-off of the lateral surface of an unnotched cylinder. The visible cracks are represented with lines of width corresponding to crack width. Using computer-tomographical analysis it was found that the cracks visible on the lateral surface also appear inside the material. The center of the concentric circular cracks is located along the longitudinal axis of the specimen, cf. Fig. 12. Such multi-axial cracking can be observed distinctly in proximity to the spallation plane. With increasing distance to the spallation plane, the diameter of the circular cracks and their width become smaller.

In the spallation experiments on notched cylinders, the specimens could be carried through to complete fragmentation with sufficient energy. These specimens show similar multiple cracking, with the primary crack orthogonal to the loading direction and the secondary cracks both orthogonal and parallel to the loading direction. Fig. 13 illustrates the wind-off of a notched

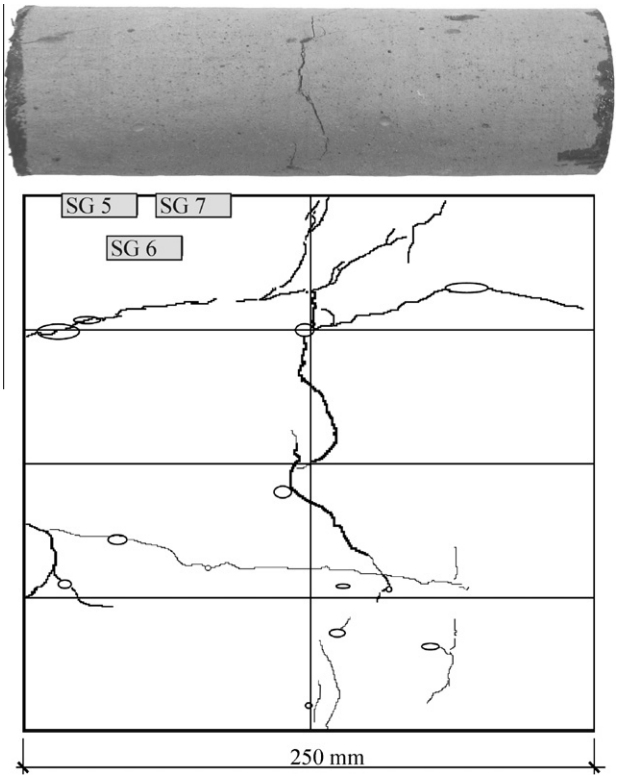

Fig. 11. Crack pattern and wind-off of crack pattern of an unnotched SHCC cylinder after Hopkinson bar experiment.

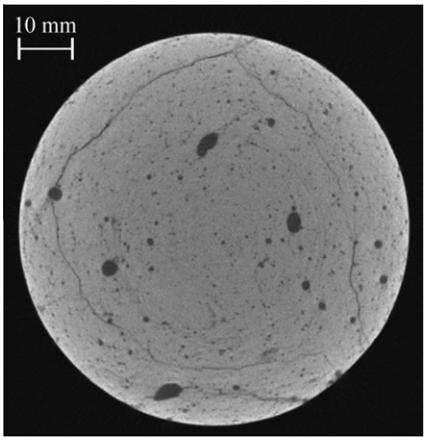

Fig. 12. Computer tomography image of an unnotched SHCC cylinder after spall experiment: circular cracking parallel to load direction.

specimen following dynamic loading. The main crack leading to the specimen failure appears in the spallation plane defined by the notch. In comparison to the experiments on unnotched SHCC specimens, fewer cracks parallel to the loading direction were observed.

4. Assessment of the results and discussion

4.1. Discussion of main material properties

To evaluate the performance of SHCC it appears helpful to compare its essential static and dynamic material properties to those of other types of concrete investigated by the authors in earlier

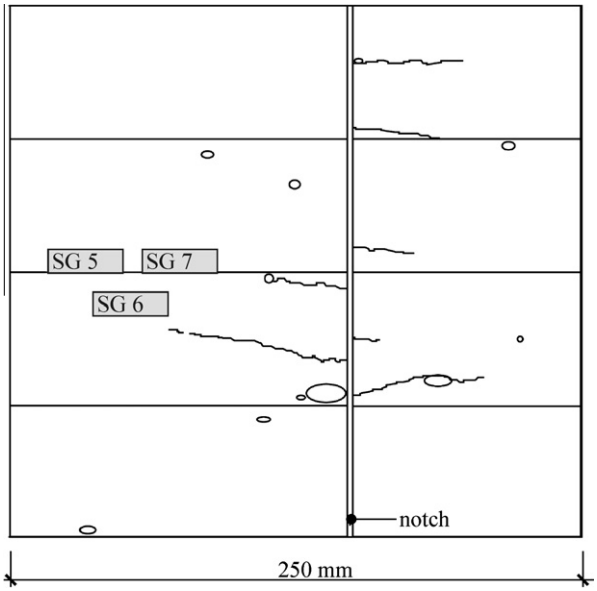

Fig. 13. Wind-off of the crack pattern of a notched SHCC cylinder after Hopkinson bar experiment.

studies: conventional (or ordinary) concrete (CC), high performance concrete (HPC) as well as ultra-high performance concrete (UHPC) with and without fibres. In comparison to conventional concrete, SHCC shows slightly better mechanical performance in terms of compressive strength (approximately 60 MPa) and tensile strength (3.8 MPa for unnotched specimens, 5.5 MPa for notched specimens) under quasi-static loading. The corresponding strength values for HPC and UHPC are higher [11,12], especially with regard to compressive strength. Young's modulus of SHCC is considerably smaller than for other concretes, including conventional concrete. First of all, this can be traced back to the absence of coarse, stiff aggregates in the SHCC mix. However, in contrast to the other types of concrete, SHCC shows quasi-ductile behaviour when subjected to tensile loading, which results from multiple cracking and effective crack-bridging by polymer fibres. Thus, in experiments on unnotched specimens total fracture energy of SHCC was 61 Nm, which is very high.

The direct comparison of this result to the behaviour of CC, HPC or UHPC is not possible since these materials require testing on notched specimens in order to record the entire stress-deformation curve and calculate the fracture energy. Unnotched specimens, when loaded under tension, would fail in an unstable manner. The total fracture energy $G_{f,stat}$ obtained from tension tests on notched SHCC specimens is at 6.69 Nm considerably lower than the corresponding value obtained for unnotched specimens. The explanation for this great difference (factor of about nine) is straightforward: the multiple cracking is not distributed over the entire length of the specimen, but is limited rather to the region in the vicinity of the notched cross-section. Furthermore, it should be noted that the area of the notched cross-section is smaller than the cross-sectional area of the unnotched specimens. The specific fracture energy $G'_{f,stat}$ for SHCC was calculated at 5561 N/m. This value is approximately 50 times higher than the specific fracture energy of conventional concrete but lower than 13,900 N/m, the value of the specific fracture energy measured for UHPC with 2.5% steel fibres [12]. The comparison to the latter value is, however, not straightforward since different specimen geometry and preparation techniques were used. The notched UHPC specimens were not core-drilled cylinders but individually cast prisms with a cross-section of 40 mm × 40 mm and two relatively wide and shallow notches (5 mm × 5 mm) positioned on two opposite sides

of the central cross-section. Wide notch and favourable fibre orientation due the casting of nearly self-compacting UHPC into a narrow mould surely have a positive effect on the mechanical performance of the hardened material. Even, so the behaviour of the notched SHCC specimens is more ductile, for the following two reasons:

(1) UHPC shows only minimal strain hardening with an increase in stress between the first-crack stress and the tensile strength of only 0.1–0.2 MPa for an average tensile strength of 9.4 MPa [12]; in contrast SHCC showed pronounced strain hardening; average first-crack stress was approximately 4.5 MPa, whereas the tensile strength was 5.53 MPa.
(2) The deformation measured on reaching tensile strength was approximately 0.2 mm for UHPC as opposed to 0.6 mm for SHCC.

However, after exceeding ultimate deformation, UHPC shows better stress transfer over the major crack in the softening regime: The complete separation of the specimen into two parts occurs at a crack opening of approximately 4.5 mm, while for SHCC this value does not exceed 2 mm.

With respect to ductility of SHCC it is also worthy of note that its tensile strength measured on notched specimens is higher than the tensile strength obtained from the experiments on unnotched specimens. Such behaviour is known also for other ductile materials, such as metals generally. For quasi-brittle materials, to which all other types of concretes considered belong, notched specimens always provide lower values of tensile strength than unnotched specimens.

For purposes of this article, however, behaviour under dynamic loading is of primary interest. Fig. 14 presents the material properties – dynamic tensile strength $f_{t,dyn}$, dynamic Young's modulus E_{dyn} and specific dynamic fracture energy $G'_{f,dyn}$ – as obtained from the spallation experiments on SHCC in comparison to conventional concrete [11] and ultra-high performance concrete with and without fibre reinforcement [12].

Similar to the results of quasi-static testing, SHCC shows no extraordinary performance regarding the tensile strength and the Young's modulus. The values of both properties increase for SHCC due to impact loading, but this is the case for CC and UHPC as well. This is again the high specific fracture energy, this time measured for impact loading regime, which is characteristic for the mechanical performance of SHCC. With a value of 13,300 N/m this property is approximately 100 times higher than that of conventional concrete. The difference to UHPC without fibre reinforcement is even more pronounced. In comparison to UHPC with a steel fibre content of 2.5%, an increase of 20% was found. This means that a higher dissipation of loading

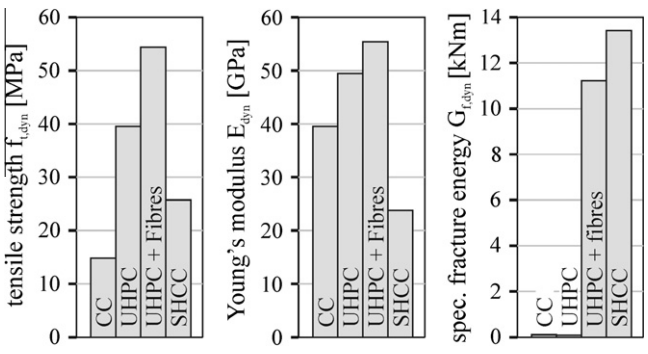

Fig. 14. Dynamic material properties of conventional concrete [11], ultra-high performance concrete (UHPC) [12] and SHCC.

energy can be accomplished by SHCC in comparison to fibre-reinforced UHPC. In contrast to the results of the quasi-static tests, the comparison of the results for SHCC and UHPC can be more straightforward since the same specimen geometry and the specimen preparation procedure was used for both types of concrete. Reasons for the superior specific fracture energy must still be investigated in more details. However, first considerations will be presented here.

The remarkable energy dissipation of SHCC can be traced back both to the particular design of the fibre–matrix bond and to its tendency to multiple crack formation, not only orthogonal to the load vector but also parallel to it. The fibre–matrix bond in SHCC is characterized by a gradual debonding process at high fibre stress levels. The effective crack-bridging by fibres delays the failure localisation and therefore supports multiple cracking in the vicinity of the notch cross-session. As was shown in [15], high-speed loading leads to the formation of a high number of finer, disconnected cracks than low speed loading does, even in the case of conventional concrete. It is likely that such increase in number of micro-cracks occurs also in SHCC under impact load, thereby activating a greater number of fibres. Similar processes are likely to occur also in UHPC with steel fibres, but to a lesser extent. Due to high tensile strength of the UHPC matrix and lower slenderness of the steel fibres (length 9 mm, diameter 0.15 mm) the bridging of the micro-cracks might be less effective than in the case of SHCC (fibre length 12 mm, diameter 0.04 mm). Both for SHCC and UHPC, it seems that due to the very brief loading time, most of these micro-cracks do not develop enough to connect to each other and form visible cracks, but this assumption is still to be proven.

Another subject to consider is that of fibre pullout. After complete debonding the fibres are pulled out from the SHCC matrix to a much larger extent than in the case of quasi-static loading (this phenomenon will be discussed in Section 4.2). Inspection of the fracture surfaces of UHPC also showed that fibre pullout occurred. However, there was a pronounced difference in the condition of the fibres: while steel fibres of UHPC showed no signs of plastic deformations, PVA fibres used for SHCC production were clearly plastically deformed. These plastic deformations may contribute considerably to the energy dissipation by SHCC under impact loading.

The next point to be addressed is the development of several cracks orthogonal to the notched cross-section in the experimentation on SHCC (cf. Figs. 11 and 12), leading to a further increase in the energy required for the spallation process. Such cracks were not observed in the corresponding tests with UHPC [12], which might be explained by its higher strength, both in tension and compression.

Finally, it should again be underlined that the specific fracture energy $G'_{f,dyn}$ was investigated on notched specimens with a predefined position of the main crack and very limited process zone volume. From the quasi-static tests it is known that unnotched specimens show much more pronounced multiple cracking and subsequently higher energy dissipation than notched specimens. Since UHPC shows a rather early localisation of failure with only very moderate strain hardening, the superiority of SHCC over UHPC in terms of its energy dissipation capacity might be even much higher if unnotched specimens could provide reliable data on the total fracture energy in impact loading regime. The development of a method for the estimation of the fracture energy from impact tests on unnotched cylinders is a subject of ongoing research by the authors.

All material properties were found to be strain-rate-sensitive, however to different extents. The strain rate effect can be described by comparison of dynamic and static values of material properties using the so-called Dynamic Increase Factor (DIF) for

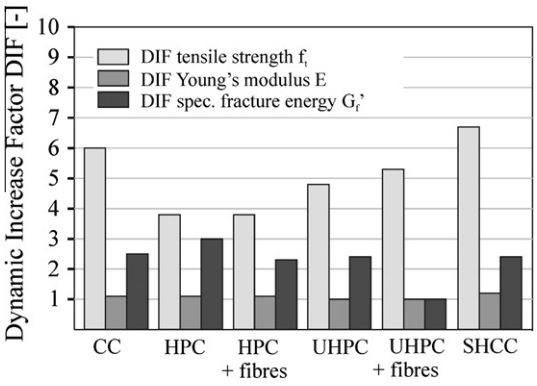

Fig. 15. DIF of different material properties of ordinary concrete [11], high performance concrete (HPC), ultra-high performance concrete (UHPC) [12] and SHCC.

quantification. The DIF is defined as quotient of the dynamic property to the corresponding static property as stated in Eq. (7). Fig. 15 presents the DIF for different types of concrete.

$$\mathrm{DIF} = \frac{X_{dyn}}{X_{stat}} \tag{7}$$

The SHCC experiments showed a pronounced strain rate effect for tensile strength with a DIF of 6.7 for unnotched specimens and 4.8 for notched cylinders, respectively. The measured strain rates were between $\dot{\varepsilon}$ 140 and 180 s^{-1}. This increase in tensile strength is comparable to the strain rate effect observed in corresponding tests on conventional and high performance concretes. The DIF of tensile strength amounted to six for conventional concrete (CC) and ranged from 3.8 for high performance concrete (HPC) to 5.3 for ultra-high performance concrete (UHPC) with fibres ($\dot{\varepsilon}$ ca. 100 s^{-1}) [12].

The strain rate dependence of Young's modulus was much less pronounced: the corresponding DIF was only 1.2 for SHCC, while for other concretes even lower DIF values or no increase in Young's modulus at all were measured.

The DIF for the specific fracture energy G_f' of SHCC was 2.4, which fits well into the range of DIF values, between 2.3 and 3 as observed for other types of concretes. The only exception is UHPC with steel fibres, whose DIF for the specific fracture energy was slightly less than 1. A partial explanation of this phenomenon may be found in this section in one of the paragraphs above, where there is a description of the differences in the specimen geometry and preparation procedure for quasi-static and dynamic tests on UHPC. It can be assumed that given the same specimen quality, the strain rate effect on the fracture energy would be observed also for UHPC.

4.2. Analysis of the specific material behaviour of SHCC under tensile loading

In the quasi-static and dynamic experiments performed, SHCC yielded multiple cracking and pronounced post cracking load transfer. Multiple cracking was observed under both loading regimens; however, the crack pattern differed considerably. In the case of quasi-static loading a number of more or less parallel cracks developed, all oriented perpendicular to the loading direction. In the dynamic tests a lesser number of visible cracks formed, some of them parallel and some perpendicular to the direction of loading. The following reasons are likely to be responsible for these particularities:

(1) In quasi-static testing the stresses are nearly evenly distributed over the specimen length. Multiple cracks form over the entire length of the specimen. This is not the case in Hopkinson bar test, where the maximum tensile stress occurs at a particular cross-section defined by the superposition of the decompression waves (cf. Section 2.5). The region of highest stress, in which cracks develop, covers only a part of the specimen.
(2) In dynamic tests SHCC specimens show cracks oriented not only perpendicular to the direction of loading but also longitudinal cracks. The latter have been never observed in quasi-static tests.
(3) As explained in Section 4.1, it is likely that during high-speed loading a great number of micro-cracks form, which probably contribute to the energy dissipation. However, these micro-cracks obviously fail to grow together to form visible cracks.

The specific behaviour of SHCC under dynamic loading manifests itself not only in the crack pattern but also in the condition of fracture surfaces. After quasi-static experiments, the visible fibre pullout lengths were between 0.2 mm and 0.5 mm (Fig. 16a and b). The fibre's surface was smooth and seemed to be the same as that of the original fibre. Many fibres failed during the crack opening along the uneven fracture surface after the fibre's tensile strength was reached (Fig. 16c).The fibre pullout lengths after dynamic loading reached values of up to 6 mm, i.e. they were manifold larger than those observed in the static experiments (Fig. 17a and b). Fibre failure due to the reaching of the fibre's tensile strength was found to be seldom. Most of the fibres showed a clearly defined cut (Fig. 17c), a result of the production process of the short fibres. The rarely visible failed fibres showed a constricted and fibrous fracture surface. The surface of many fibres which showed a long pullout length revealed significant changes in comparison to the unloaded state. In contrast to the smoothly surfaced fibres observed after quasi-static testing, fibres following dynamic testing were uneven and showed in the axial direction an irregular, wave-shaped texture indicating pronounced plastic deformations. Similar phenomena of fibre pullout were observed in uniaxial, high-speed tensile tests on SHCC in [14]. The strain rates in those tests ranged from 10^{-5} s^{-1} up to 50 s^{-1}. High speed tests were performed at strain rates of 10 s^{-1}, 25 s^{-1} and 50 s^{-1} on dumbbell shaped specimens. At strain rates up to 10^{-2} s^{-2}, decreasing ductility was observed, which is in accordance with earlier findings [3,4,6]. However, increasing ductility and energy absorption capacity were found at strain rates equal or higher than 10 s^{-1}.

The changes in the fibre surface show that the fibres are particularly subject to plastic deformations at high strain and high crack-opening velocities. It is assumed that in such load cases the bond between fibre and interfacial transition zone of the matrix is damaged, thus favouring fibre pullout. The expected more brittle behaviour of the fibre pullout with increased strain rate, resulting from an increase in the bond strength of the fibre–matrix interaction [3,6], as proven at low strain rates, seems to be more than compensated by this effect. Further investigations are necessary to explain the phenomena of material failure at high strain rates leading to the positive mechanical characteristics during impact loading. In particular questions of crack initiation, of crack growth, and also of the processes related to fibre pullout and failure must be answered.

Answering these questions is of particular importance, especially with regard to the purposeful material design of SHCC for particular applications. The following deliberations over the development and testing of the SHCC material presented in this study should give a rough idea about the particularities of such a task.

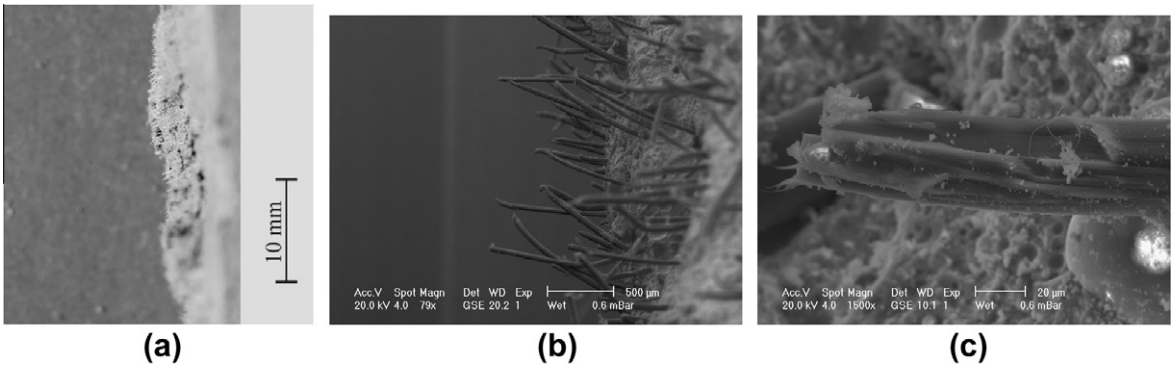

Fig. 16. Pullout lengths of fibres under quasi-static loading (a and b), typical shape of fibre fracture (c).

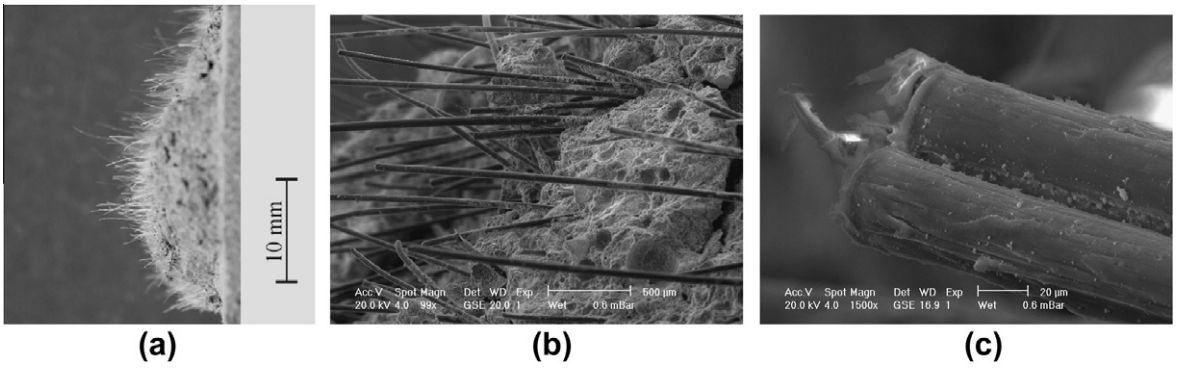

Fig. 17. Pullout lengths of fibres under high dynamic loading (a and b), typical shape of pulled-out fibres (c).

SHCC is usually designed such that the fibres spanning a crack first gradually debond from the matrix, still remaining anchored at the ends. Increasing the free length of the fibres is requisite to the high deformability of the fibres themselves and, consequently, to the controlled opening of the corresponding crack and the large deformations which result from the opening of a great number of cracks. Since the position and orientation of individual fibres related to the crack plane are different (the anchoring length may vary between zero and half of the fibre length), compete debonding from the matrix occurs for different fibres at different stages of loading. With localisation of the failure at the weakest crack plane, most of the fibres are pulled out of the matrix, while some fibres, predominantly those with a longer anchoring length and oriented non-perpendicular to the crack plane, fail. Ductile material behaviour is associated with pronounced fibre pullout and only few broken fibres at the fracture surface.

The material design for the SHCC under investigation was conceived in such a way that the fibres were predominantly pulled out [7]. However, the testing associated with development of the mix differed from that used in this study. That led to performance of the material under quasi-static loading different to that described in Section 3.1. In the present study the cylinders were core-drilled from a large block. Thus, the fibres in core-drilled cylinders were randomly oriented and cut at the cylinder surface. In contrast to this, the surfaces of the dumbbell shaped specimens used in [7] were defined by the formwork geometry. Here no fibres were cut and the fibre orientation at the specimen surface was parallel to the surface and hence aligned with the loading direction. Furthermore, the dumbbell specimens had the rather slender cross-section of only 40 mm $\times$ 24 mm, which also influenced the orientation of the fibres in the direction of loading. Consequently in the majority of cases in the tests on dumbbell specimens, more favourably oriented fibres tended to be pulled out nearly independently of the anchoring length. Contrastingly in the cylindrical specimens used in this study the fibres were randomly distributed. With increasing deviation of the fibre orientation from the direction parallel to tensile loading and perpendicular to crack plane, the anchoring of the fibre in the matrix is improved and the debonding and pullout resistances increase [16]. As a result the failure probability of fibres with longer embedded lengths increased, and only fibres with shorter embedment lengths can be pulled out of the matrix. Thus, these short pullout fibre lengths dominated the appearance of the fracture surfaces of the tested cylinders in quasi-static tests, cf. Fig. 16b.

With increasing strain rates a decrease in the number of cracks and an increase in the probability of fibre failure were observed in previous studies, accompanied by decreasing average fibre pullout length [3,4,14]. However, this tendency seems to be valid for a quasi-static regime only. In this study, as well as in [14], a cardinal change in the failure mode was observed under impact loading: very pronounced fibre pullout occurred unexpectedly.

From the above it can be concluded that SHCC material design can and should to be adjusted depending on the expected loading rates. Furthermore, particular attention should be given to specimen geometry and preparation methods as well as to testing procedures. The testing should reflect as far as possible the conditions in structural members under consideration.

5. Summary and outlook

This paper presents the results of static and dynamic experimental investigations on strain hardening cement-based composite (SHCC). Spallation experiments were performed using a Hopkinson bar device to investigate the dynamic properties of SHCC.

Under static loading SHCC shows decidedly ductile behaviour due to the formation of multiple cracks and the crack-bridging by PVA short fibres. The energy absorption capacity of SHCC is very high, especially when unnotched specimens are considered. The specific fracture energy obtained from the tests on notched specimens amounts to 5500 N/m, which is approximately 50 times higher than that of conventional concrete.

Dynamic experiments on the Hopkinson bar show that the positive material characteristics, like the pronounced quasi-ductile behaviour and high energy absorption capacity as observed under quasi-static loading remained and even improved with loading at high strain rates. A significant strain rate effect for the tensile strength (Dynamic Increase Factor DIF = 6.7) and a more moderate effect in the case of fracture energy (DIF = 2.4) were measured. The reasons for this increase in the performance at high strain rates are assumed to be related to the development of a great number of micro-cracks parallel with and orthogonal to the loading direction and to the extensive plastic deformations of fibres prior to and during fibre pullout. The predominant fibre pullout in the dynamic tensile tests was unexpected since previous investigations showed an increase of fibre failure probability with increasing strain rate. Those results, however, were obtained for a quasi-static loading regime. Obviously the failure mechanisms of SHCC are altered when impact loading is applied. This phenomenon should be investigated in more details.

In dynamic loading, SHCC shows superior performance with regard to fracture energy when compared to conventional, high-performance or ultra-high-performance concrete with or without fibres. The strain rate effect on the tensile strength of SHCC was found to be more pronounced than on other types of concrete. The Dynamic Increase Factor of fracture energy was similar to the corresponding values for other concretes. In consideration of the total fracture energy (work to fracture), the beneficial behaviour of SHCC should be even more distinct. However, this material property cannot be measured using the methods described in the article. Further investigations should attempt better to understand multiple cracking in dynamic experiments using modified test methods.

In addition to developing an experimental configuration for determining total fracture energy, measuring stress–strain relations under conditions of dynamic loading is essential to a complete understanding of material behaviour. It is a challenging task. Furthermore, the matrix-fibre interaction should be analyzed with the help of dynamic pullout experiments. The general goal of future investigations by the authors along this line is the development of a concept for increasing the resistance of brittle cementitious materials in the case of dynamic loads with the help of short, ductile polymer fibres.

References

[1] Li VC. On engineered cementitious composites (ECC): a review of the material and its applications. J Adv Concr Technol 2003;1(3):215–30.

[2] Mechtcherine V, Schulze J. Ultra-ductile concrete–material design concept and testing. CPI Concr Plant Int 2005;5:88–98.

[3] Yang E, Li VC. Rate dependence in engineered cementitious composites. In: Int RILEM workshop on HPFRCC in structural applications, vol. 49. RILEM Publications S.A.R.L., PRO; 2005. p. 83–92.

[4] Douglas KS, Billington SL. Rate dependence in high-performance fiber reinforced cementbased composites for seismic applications. In: Int RILEM workshop on HPFRCC in structural applications, vol. 49. RILEM Publications S.A.R.L., PRO; 2005. p. 17–26.

[5] Maalej M, Zhang J, Quek ST, Lee SC. High-velocity impact resistance of hybridfiber engineered cementitious composites. In: Proc of the 5th int conf on fracture mechanics of concrete and concrete structures (FraMCoS-5), vol. 4; 2004. p. 1051–8.

[6] Boshoff WP, Mechtcherine V, van Zijl GPAG. Characterising the time-dependant behaviour on the single fibre level of SHCC: part 2: The rate effects on fibre pull-out test. Cem Concr Res 2009;39:787–97.

[7] Brüdern A-E, Mechtcherine V. Multifunctional use of SAP in Strain-hardening Cement-based Composites. In: Int RILEM conference on use of superabsorbent polymers and other new additives in concrete, Technical University of Denmark, Lyngby, RILEM PRO, vol. 74; 2010. p. 11–22.

[8] Weerheijm J. Concrete under impact tensile loading and lateral compression, Delft University of Technology. Dissertation; 1992.

[9] Schuler H. Experimentelle und numerische Untersuchungen zur Schädigung von stoßbeanspruchtem Beton. epsilon – Forschungsergebnisse aus der Kurzzeitdynamik, Heft 6, Freiburg im Breisgau: Fraunhofer Institut für Kurzzeitdynamik, EMI 2004, ISBN 3-8167-6463-0.

[10] Millon O, Nöldgen M, Riedel W, Thoma K, Fehling E. Fiber-reinforced ultra-high performance concrete under tensile loads. In: 9th Int conf on the mechanical and physical behaviour of materials under dynamic loading. Brussels: EDP Sciences; 2009.

[11] Schuler H, Mayrhofer C, Thoma K. Spall experiments for the measurement of the tensile strength and fracture energy of concrete at high strain rates. Int J Impact Eng 2006;32:1635–50.

[12] Nöldgen M, Millon O, Thoma K, Fehling E. Hochdynamische Materialeigenschaften von Ultrahochleistungsbeton(UHPC). Beton und Stahlbetonbau 2009;104:717–26.

[13] Mechtcherine V. Testing behaviour of strain hardening cement-based composites in tension – summary of recent research. In: Reinhardt H-W, Naaman A, editors. RILEM-symposium on high-performance fibre reinforced cementitious composites HPFRCC5. RILEM PRO, vol. 53; 2007. p. 13–22.

[14] Silva FA, Butler M, Mechtcherine V, Zhu D, Mobasher B. Mechanical behaviour of strain-hardening cement-based composites (shcc) under low and high tensile strain rates. In: Mechtcherine V, Kalsike M, editors. Fracture and damage of advanced fibre-reinforced cement-based materials. Freiburg: Aedificatio Publishers; 2010. p. 23–30.

[15] Mechtcherine V. Fracture mechanical behaviour of concrete and the condition of its fracture surface. Cem Concr Res 2009;39:620–8.

[16] Jun P, Mechtcherine V. Behaviour of strain-hardening cement-based composites (SHCC) under monotonic and cyclic tensile loading: part 2 – modelling. Cem Concr Compos 2010;32:810–8.